RESEARCH ARTICLE

MHC-I and PD-L1 Expression is Associated with Decreased Tumor Outgrowth and is Radiotherapy-inducible in the Murine Head and Neck Squamous Cell Carcinoma Model MOC1

Daan F. Boreel[1,2] · Gerwin G. W. Sandker[2] · Marleen Ansems[1] · Renske J. E. van den Bijgaart[1] · Johannes P. W. Peters[1] · Paul N. Span[1] · Gosse J. Adema[1] · Sandra Heskamp[2] · Johan Bussink[1]

Abstract

Introduction Combined radiotherapy and immune checkpoint inhibition is a potential treatment option for head and neck squamous cell carcinoma (HNSCC). Immunocompetent mouse models can help to successfully develop radio- immuno- therapy combinations and to increase our understanding of the effects of radiotherapy on the tumor microenvironment for future clinical translation. Therefore, the aim of this study was to develop a homogeneous, reproducible HNSCC model originating from the Mouse Oral Cancer 1 (MOC1) HNSCC cell line, and to explore the radiotherapy-induced changes in its tumor microenvironment, using flow cytometry and PD-L1 microSPECT/CT imaging.

Materials and Methods *In vivo* growing tumors originating from the parental MOC1 line were used to generate single cell derived clones. These clones were screened *in vitro* for their ability to induce programmed cell death ligand 1 (PD-L1) and major histocompatibility complex class I (MHC-I) following IFNγ exposure. Clones with different IFNγ sensitivity were inoculated in C57BL/6 mice and assessed for tumor outgrowth. The composition of the tumor microenvironment of a stably growing (non)irradiated MOC1-derived clone was assessed by immunohistochemistry, flow cytometry and PD-L1 microSPECT/CT.

Results Low *in vitro* inducibility of MHC-I and PD-L1 by IFNγ was associated with increased tumor outgrowth of MOC1 clones *in vivo*. Flow cytometry analysis of cells derived from a stable *in vivo* growing MOC1 clone MOC1.3D5^{low} showed expression of MHC-I and PD-L1 on several cell populations within the tumor. Upon irradiation, MHC-I and PD-L1 increased on leukocytes (CD45.2$^+$) and cancer associated fibroblasts (CD45.2$^-$/EpCAM$^-$/CD90.1$^+$). Furthermore, PD-L1 micro- SPECT/CT showed increased tumor uptake of radiolabeled PD-L1 antibodies with a heterogeneous spatial distribution of the radio signal, which co-localized with PD-L1$^+$ and CD45.2$^+$ areas.

Discussion PD-L1 and MHC-I inducibility by IFNγ *in vitro* is associated with tumor outgrowth of MOC1 clones *in vivo*. In tumors originating from a stably growing MOC1-derived clone, expression of these immune-related markers was induced by irradiation shown by flow cytometry on several cell populations within the tumor microenvironment such as immune cells and cancer associated fibroblasts. PD-L1 microSPECT/CT showed increased tumor uptake following radiotherapy, and autoradiography showed correlation of uptake with areas that are heavily infiltrated by immune cells. Knowledge of radiotherapy-induced effects on the tumor microenvironment in this model can help optimize timing and dosage for radio- immunotherapy combination strategies in future research.

Keywords Radiotherapy · Immunotherapy · HNSCC · Tumor microenvironment

---

✉ Daan F. Boreel
daan.boreel@radboudumc.nl

1   Radiotherapy and OncoImmunology Laboratory, Department of Radiation Oncology, Radboudumc, Geert Grooteplein Zuid 32, 6525GA Nijmegen, The Netherlands

2   Department of Medical Imaging, Radboudumc, Geert Grooteplein 10, Nijmegen 6525GA, The Netherlands

Introduction

Head and neck cancer is the seventh most common cancer worldwide of which head and neck squamous cell carcinoma (HNSCC) comprises the majority of patients [1]. HNSCC includes cancers of the larynx, pharynx, and oral cavity [2]. Most patients are diagnosed at late stages, presenting with locally advanced disease, and have a poor prognosis

[1]. Combining radiotherapy with immune checkpoint inhibition holds potential as a curative treatment option due to the anti-tumor immune-enhancing effects of irradiation [3]. However, the combination of radiotherapy with inhibition of programmed cell death protein (PD-1) or its ligand 1 (PD-L1) has not proven to be effective yet for HNSCC patients and several trials are currently ongoing [4–8]. Possible mechanisms contributing to the ineffectiveness of current radio- immunotherapy approaches in HNSCC might be related to dampening of the immune response by elective nodal irradiation or therapy timing [9, 10].

Preclinical studies have indicated that radiotherapy-immunotherapy combinations may be more effective than monotherapies [11–14]. Other studies suggest that additional modulation of the tumor microenvironment (TME) might be necessary to achieve the full potential of these combined treatments [15–19]. To better understand the potential synergistic effects of radiotherapy and immune checkpoint inhibition, in-depth mechanistic studies in preclinical syngeneic HNSCC tumor models are needed. For instance, the evolving TME -including immune cells and cancer associated fibroblasts (CAFs)- is known to play an important role in tumor growth and progression [19–21]. Moreover, expression of immune-related markers upregulated by Interferon gamma (IFNγ) signaling like PD-L1 and major histocompatibility complex class I (MHC-I) in the TME, i.e. on non-tumor cells, have been linked to improved prognosis and reduced tumor outgrowth, although some contradictory reports exist [22–27]. Understanding of immune response-related markers and the radiation-induced effects on them are necessary to determine the optimal timing, response prediction, and/or sensitization to radio- immunotherapy combinations in HNSCC.

Only a limited number of murine HNSCC models are available and the most well-studied one is murine oral cancer 1 (MOC1), which has been used before to demonstrate the efficacy of radio- immunotherapy combination strategies [11, 28, 29].

In this study, we aim to develop a homogeneous, reproducible HNSCC model of MOC1 origin after *in vivo* passage of the parental MOC1 cells, selected based on IFNγ-inducibility of immunological markers MHC-I and PD-L1. Furthermore, we aim to explore radiotherapy-induced changes in the TME of this tumor model. Using single-cell-derived clones, we showed that *in vitro* MHC-I and PD-L1 expression was associated with *in vivo* tumor outgrowth. Additionally, in the selected MOC1 clone, radiotherapy-induced expression of MHC-I on leukocytes and PD-L1 on leukocytes and CAFs *in vivo*. By PD-L1 microSPECT/CT, an increased tumor uptake was measured following radiotherapy. This knowledge will contribute to optimizing the efficacy of radio- immunotherapy combinations in HNSCC.

Material and Methods

Cell Lines

MOC1 (provided by R. Uppaluri, Dana-Farber Cancer Institute, Boston) cells or single cell-derived MOC1 clones were cultured in 2:3 Iscove's Modified Dulbeco's Medium, 1:3 Ham's F-12 nutrient mix with 5% Fetal Calf Serum, 1% penicillin–streptomycin (all Gibco), 5 ng/mL Epidermal Growth Factor (EMD Millipore), 40 ng/mL hydrocortisone and 5 µg/mL insulin (both Sigma Aldrich) at 37 °C in 5% CO_2 and 20% O_2. Cells were stimulated with recombinant murine IFNγ (5 ng/mL) (Peprotech) for 24 h. For *in vitro* experiments, cells were not passaged more than fifteen times post thawing. For *in vivo* experiments, cells were passaged two times post thawing.

Mice

All animal experiments were conducted in accordance with the principles laid out by the Dutch Act on Animal Experiments (2014) and approved by the Animal Welfare Body of the Radboud University Nijmegen and Central Authority for Scientific Procedures on Animals. In all animal experiments, female C57BL/6 mice that can be housed together in groups (10–12 weeks, Charles River) were used. Mice were housed in individually ventilated cages with filter top (IVC Blueline, Tecniplast) and could eat and drink ad libitum. In all experiments animals were assigned to groups by block randomization based on tumor volume. Tumor size was determined by caliper measurement by biotechnicians that were blinded to experimental groups. Tumor volume was calculated using the following formula:

$$Tumor\ volume = Height \times Width^2 \times 0.5$$

Fluorescence-Activated Cell Sorting of *In Vivo* Passaged Tumor Cells

Mice were subcutaneously (s.c.) inoculated with 0.5×10^6 or 1.0×10^6 MOC1 cells in phosphate buffered saline (PBS) on the right hindleg to monitor tumor growth (n = 3 per group). At day 57 post injection mice were sacrificed and tumors were excised, mechanically dissociated in Serum Free RPMI (Gibco) with 1 mg/mL collagenase type III (Worthington) and 30 µg/mL DNase type I (Roche), and incubated for 30 min at 37 °C. EDTA was added to a final concentration of 1 mM and cells were passaged twice over an 100 µm cell strainer (BD Falcon) to retrieve a single cell suspension. 1.0×10^6 cells were seeded in a T75 culture

flask (Corning) and expanded. For fluorescence-activated cell sorting cells were harvested and incubated for 15 min at 4 °C with rat anti-EpCAM-FITC (1:400, eBioscience). EpCAM-positive cells were sorted as single cells using a FACSAria II SORP sorter (BD Bioscience) and further expanded *in vitro*.

In vitro Radiosensitivity and Cell Growth

To assess radiosensitivity, colony-forming assays were performed as previously described using a 320 kV Xrad irradiator (RPS Services Limited) at a dose rate of 3.8 Gy/min [30]. *In vitro* cell growth was measured using the IncuCyte ZOOM Live-Cell Analysis System (Essen BioScience). For MOC1 parental or MOC1 clones, 500 cells/well were seeded in 96-wells plates (Corning). Images were retrieved and confluency was calculated as previously described [31]. No differences in cell viability were observed. Doubling time was calculated using the following formula:

$$Doubling\ time = \frac{Time \times \log(2)}{(\log(Final\ confluency) - \log(Initial\ confluency))}$$

Comparison of MOC1 Clone's Outgrowth

MOC1 clones were selected based on the inducibility by IFNγ of MHC-I and PD-L1; 3D5 (MOC1.3D5^{low}), 4E8 (MOC1.4E8^{intermediate}), 4B9 (MOC1.4B9^{high}). To compare tumor growth of MOC1 clones, mice were inoculated s.c. with 0.5×10^6 cells of MOC1.3D5^{low}, MOC1.4E8^{intermediate}, MOC1.4B9^{high} and MOC1 parental in 1:3 matrigel (BD Bioscience): PBS on the right hindleg (n = 5 per group). Mice were sacrificed when tumors reached a size of approximately 400 mm^3. Half of the tumor was dissociated for flow cytometry analysis as described above, and half of the tumor was snap-frozen in liquid nitrogen for immunohistochemistry (IHC) analyses.

Antibodies and Flow Cytometry Analysis

Single cell suspension harvested from *in vitro* cultured cells, or single cell suspension of *in vivo* grown tumors were used. Cells were incubated with viability dye eFluor™ 780 or eFluor™ 450 (eBioscience) in PBS for 15 min at 4 °C to distinguish living and dead cells. Before staining cells were washed twice in 0.5% serum albumin and 0.05% sodium azide in PBS (PBA) and incubated with anti-CD16/CD32 Fc-block (BD) for 15 min at 4 °C. Cells were washed twice in PBA and stained for 30 min at 4 °C using the following antibodies or appropriate isotype controls: CD90.2-BV510 (Thy-1.2), MHC-I-PE (H-2 Kb/H-2D^b), CD45.2-A647 (Ly5.2), Ly6G-BV605, CD3-BV510, CD45.2-PerCP/Cy5.5 (Ly5.2), IgG2b,

k-BV510, IgG2a, k-PE, IgG2a, k-PE/Cy7, IgG2a, k-APC from Biolegend, PD-L1-APC (CD274), CD11c-BUV395 (ITGAX), CD11b-BUV737 (ITGAM), Ly6C-A700 from BD Bioscience, EpCAM-FITC (CD326), PD-L1-PE/Cy7 (CD274), CD25-APC (IL2RA), FoxP3-PE/Cy7 from eBioscience and CD45.2-FITC (Ly5.2), F4/80-PE/Cy7 (EMR1), CD4-APC/Cy7, CD8β.2-FITC (Ly-3), NK1.1-PE from Antibodychain. After staining cells were washed in PBA and measured on the FACSCantoII (BD) or Cyto-FLEX LX Flow Cytometer (Beckman Coulter). Data were analyzed using FlowJo V10.7 (Tree Star) as previously described [32].

Irradiation of Mice for Flow Cytometry Analysis

For further characterization we selected clone MOC1.3D5^{low}, which consistently grew out into solid tumors. To determine effects of irradiation on the TME, MOC1.3D5^{low} cells were inoculated on the right hindleg and when tumors reached a size of 200 mm^3 were irradiated with a single dose of 6, 10 or 18 Gy using a 320 kV Xrad irradiator at a dose rate of 3.8 Gy/min or received no irradiation. To ensure irradiation of only the tumor-bearing right hindleg the rest of the mice body was shielded by lead. Tumors were harvested at 3 (n = 6 per group) and 10 (n = 3 per group) days post irradiation and dissociated for flow cytometry analysis as described above.

PD-L1 microSPECT/CT Imaging of (Non-)irradiated Mice

MOC1.3D5^{low} cells were inoculated on the right hindleg and when tumors reached a size of 200 mm^3, tumors were irradiated with a single dose of 10 Gy using a 320 kV Xrad irradiator at a dose rate of 3.8 Gy/min ([^{111}In]In–anti–mPD-L1 group), with a clinical 10 MV photon beam at a dose rate of 6 Gy/min (Elekta) ([^{111}In]In-IgG2b group) or received no irradiation (n = 6 per group). Rat anti-mPD-L1 (clone 10F.9G2, Bio X Cell) or rat IgG2b (clone LTF-2, Bio X Cell) was labeled with Indium-111 (^{111}In) as previously described [33, 34]. 24 h post irradiation mice received 30 µg [^{111}In]In–anti–mPD-L1 (0.48 MBq/µg) or 30 µg [^{111}In]In-IgG2b (0.53 MBq/µg) intravenously in the tail vein. 24 h-post tracer administration SPECT/CT images were acquired with the U-SPECT-II/CT system (MILabs). Mice were scanned using the following acquisition settings: 30 min acquisition time, 1.0 mm-diameter pinhole mouse high sensitivity collimator, and CT parameters of 160-µm spatial resolution, 615 µA, and 65 kV. Data were reconstructed using the MILabs software (version 2.04) using the following settings: energy windows at 171 keV (range 154 to 188 keV) and 245 keV (range 220 to 270 keV), 1 iteration, 16

subsets, and a 0.4 mm voxel size. Maximum intensity projections were created using VivoQuant. After SPECT/CT imaging mice were dissected, tumor and selected organs were weighed and radioactivity was measured using a γ-counter (2480 Wizard, Perkin-Elmer). Results are presented as percentage injected dose per gram tissue (%ID/g). Tumors were snap-frozen in liquid nitrogen for IHC analyses.

Immunohistochemistry and Autoradiography

For IHC analyses, frozen tumors were sectioned (5 μm), mounted on poly-ʟ-lysine coated slides and fixed in ice-cold acetone for 10 min. For the IHC staining, sections were blocked with 5% normal donkey serum (30 min, RT) (Jackson ImmunoResearch) and incubated (30 min, 37 °C) with rat anti-MHC-I (1:200, Invitrogen), goat anti-PD-L1 (1:100, Biotechne), biotinylated rat anti-EpCAM (1:200, Invitrogen), biotinylated mouse anti-CD45.2 (1:100, Biolegend), biotinylated rat anti-MHC-II (1:200, Antibodychain) or 9F1 against mouse vessels (Radboudumc). Subsequently, secondary antibodies were applied (45 min, 37 °C); for MHC-I chicken anti-rat Alexa647 (1:100, Invitrogen), for PD-L1 donkey anti-goat F(ab')$_2$ fragment Cy3 (1:300, Jackson Immunoresearch) or donkey anti-goat Alexa488 (1:600, Invitrogen), for EpCAM chicken anti-rat Alexa647 (1:100, for CD45.2 donkey anti-mouse F(ab')$_2$ fragment Alexa488 (1:100, Jackson ImmunoResearch) or mouse anti-biotin Cy3 (1:100, Jackson ImmunoResearch), for MHC-II mouse anti-biotin Cy3 (1:100) and for 9F1 chicken anti-rat Alexa647 (1:100). Whole-tissue section gray-scale images (pixel size, 2.59×2.59 μm) MHC-I, PD-L1, EpCAM and CD45.2 were obtained as previously described [35]. For Autoradiography (AR), frozen tumor sections (5 μm) of mice injected with [^{111}In]In–anti–mPD-L1 were mounted on poly-ʟ-lysine coated slides and exposed to a Fujifilm BAS 2025 photosensitive plate (Fuji Photo Film). Plates were scanned using an AS-1800 II bioimaging analyzer at a pixel size of 25×25 μm. AR images were analyzed using Aida Image Analyzer software (Raytest). Spatial correlation between IHC and AR images was assessed as previously described [36].

Statistical Analysis

Statistical analyses were performed using GraphPad Prism (version 8.0). Results are expressed as mean $\pm$ SD unless indicated otherwise. Unpaired t-test was used to compare 2 groups. One-way ANOVA was used to compare > 2 groups. A chi-squared test was used to compare tumor outgrowth between groups. A spearman test was used to

assess correlations between values. p values of 0.05 or less were considered significant.

Results

Characterization of Single Cell-derived MOC1 Clones

MOC1 parental cells inoculated on the right hindleg of C57BL/6 mice showed heterogenous tumor outgrowth *in vivo,* irrespective of the implantation protocols used (i.e. tumor cell suspension in PBS or Matrigel) (Supplementary Fig. S1). To develop a syngeneic mouse model with a more predictable tumor growth, a MOC1 tumor was dissociated into single cells and re-plated to obtain MOC1 clones with reproducible and homogeneous tumor growth *in vivo*. Hereto, the tumor cells were single cell-sorted by their expression of epithelial cell adhesion molecule (EpCAM). Subsequent flow cytometry analysis of 44 different MOC1 clones plus the MOC1 parental cell line revealed a great heterogeneity in their IFNγ inducibility of PD-L1 and MHC-I expression (data not shown). Based on these findings, a high-inducible (MOC.4B9^{high}), intermediate-inducible (MOC1.4E8^{intermediate}) and low-inducible (MOC1.3D5^{low}) clone were selected (Fig. 1A-B). Clones that were high-inducible for PD-L1 expression were also high-inducible for MHC-I expression and vice versa. Additional characterization of these MOC1 clones revealed a similar *in vitro* doubling time for all clones (MOC1.3D5^{low} = 15.95 ± 0.45 h, MOC1.4E8^{intermediate} = 15.87 ± 0.36 h, MOC1.4B9^{high} = 15.48 ± 0.25 h), which was significantly longer compared to the MOC1 parental cell line (12.23 ± 0.47 h, p = 0.0001) (Fig. 1C). Importantly, irradiation of MOC1 clones showed no significant differences in the surviving fraction between the MOC1 parental cell line and the clones (Fig. 1D).

Tumor Outgrowth of Single Cell-derived MOC1 Clones is Associated with MHC-I and PD-L1 Expression and Inducibility

To compare *in vivo* tumor outgrowth of MOC1 clones, mice were inoculated with the MOC1 parental, MOC1.4B9^{high}, MOC1.4E8^{intermediate} or MOC1.3D5^{low} cells on the right hindleg. Tumor outgrowth rates were significantly different between the different clones (p = 0.02) (Fig. 2A). We observed no differences in the presence of several subsets of myeloid cells (CD11b$^+$, F4/80$^+$, CD11c$^+$, Ly6G$^+$ and Ly6C$^+$) and lymphocytes (NK1.1$^+$, CD3$^+$, CD8$^+$, CD4$^+$ and Tregs) (Supplementary Fig. S2 and S3) in the TME of the different sub-clones as well as the MOC1 parental cell line. IHC analysis of the tumor
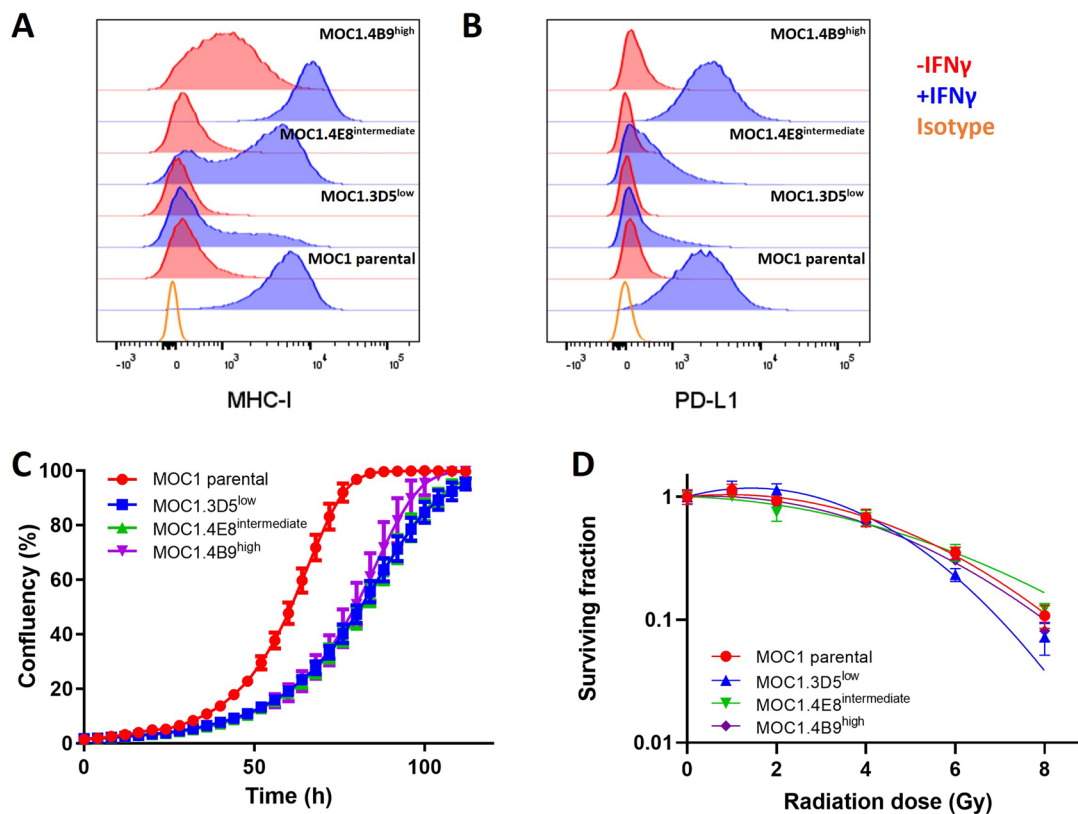
Fig. 1 *In vitro* characterization of MOC1 parental cells and MOC1 clones. (**A**) MHC-I expression and (**B**) PD-L1 expression of MOC1 parental, MOC1.4B9^{high}, MOC1.4E8^{intermediate} and MOC1.3D5^{low}, unstimulated or treated with IFNγ (5 ng/mL, 24 h). Typical example of 3 independent experiments. (**C**) *In vitro* growth curves of MOC1 parental, MOC1.4B9^{high}, MOC1.4E8^{intermediate} and MOC1.3D5^{low}. (**D**) *In vitro* radiosensitivity of MOC1 parental, MOC1.4B9^{high}, MOC1.4E8^{intermediate} and MOC1.3D5^{low}. Graph C and D show mean ± SD

tissue for MHC-I and PD-L1 expression showed a significantly increased mean optical density for MHC-I in MOC1.4E8^{intermediate} compared MOC1.3D5^{low} (p = 0.007) and MOC1 parental tumors (p = 0.008) (Fig. 2B and supplementary Fig. S4). A similar trend was observed for the mean optical density of PD-L1 (Fig. 2C). These findings suggest that the lower *in vitro* observed inducibility of MHC-I and PD-L1 of MOC1.3D5^{low} was retained *in vivo* and may have a role in tumor outgrowth.

Radiotherapy Induces Upregulation of MHC-I and PD-L1 Expression on Several Cell Populations within the Tumor Microenvironment of MOC1.3D5^{low}

To investigate whether irradiation also influences expression of these factors on tumor cells and other cell populations within the TME, mice bearing stably growing MOC1.3D5^{low} tumors were irradiated with 6, 10 or 18 Gy. The TME was analyzed by flow cytometry at 3 and 10 days post-irradiation to compare early effects with

effects occurring at a later stage. The dose range chosen is similar to the biological effective dose of earlier studies investigating fractionated radiotherapy [11]. Tumor volume was significantly reduced in mice irradiated with 10 Gy (p = 0.008) or 18 Gy (p = 0.005) at 10 days post irradiation (Fig. 3A). Flow cytometry analysis of the TME revealed both PD-L1 and MHC-I expression on CD45$^+$ leukocytes, CD45.2$^-$/EpCAM$^+$ tumor cells and CD45.2$^-$/EpCAM$^-$/CD90.1$^+$ CAFs (Fig. 3B-C). Moreover, irradiation of the tumor induced a dose dependent upregulation of PD-L1 on leukocytes and CAFs at 3 and 10 post irradiation, and a significant upregulation of MHC-I expression on leukocytes at 3 days post irradiation (Fig. 3B-C). The percentage PD-L1 and MHC-I-positive cells of the parent populations are provided in Supplementary Figure S5 and showed an additional increase of PD-L1-positive EpCAM$^+$ tumor cells at 10 days post irradiation. Increase of PD-L1 and MHC-I gMFI on MOC1.3D5^{low} tumor cells was also observed *in vitro* at 24 h post irradiation, although isotype control staining also slightly increased (Supplementary Fig. S6).

Fig. 2 *In vivo* tumor outgrowth is associated with decreased PD-L1 and MHC-I inducibility *in vitro* and expression *in vivo* (**A**) Tumor growth of MOC1 parental, MOC1.4B9[high], MOC1.4E8[intermediate], and MOC1.3D5[low] (**B**) Mean optical density of tumor sections stained for MHC-I. (**C**) Mean optical density of tumor sections stained for PD-L1. All graph bars show mean ± SD
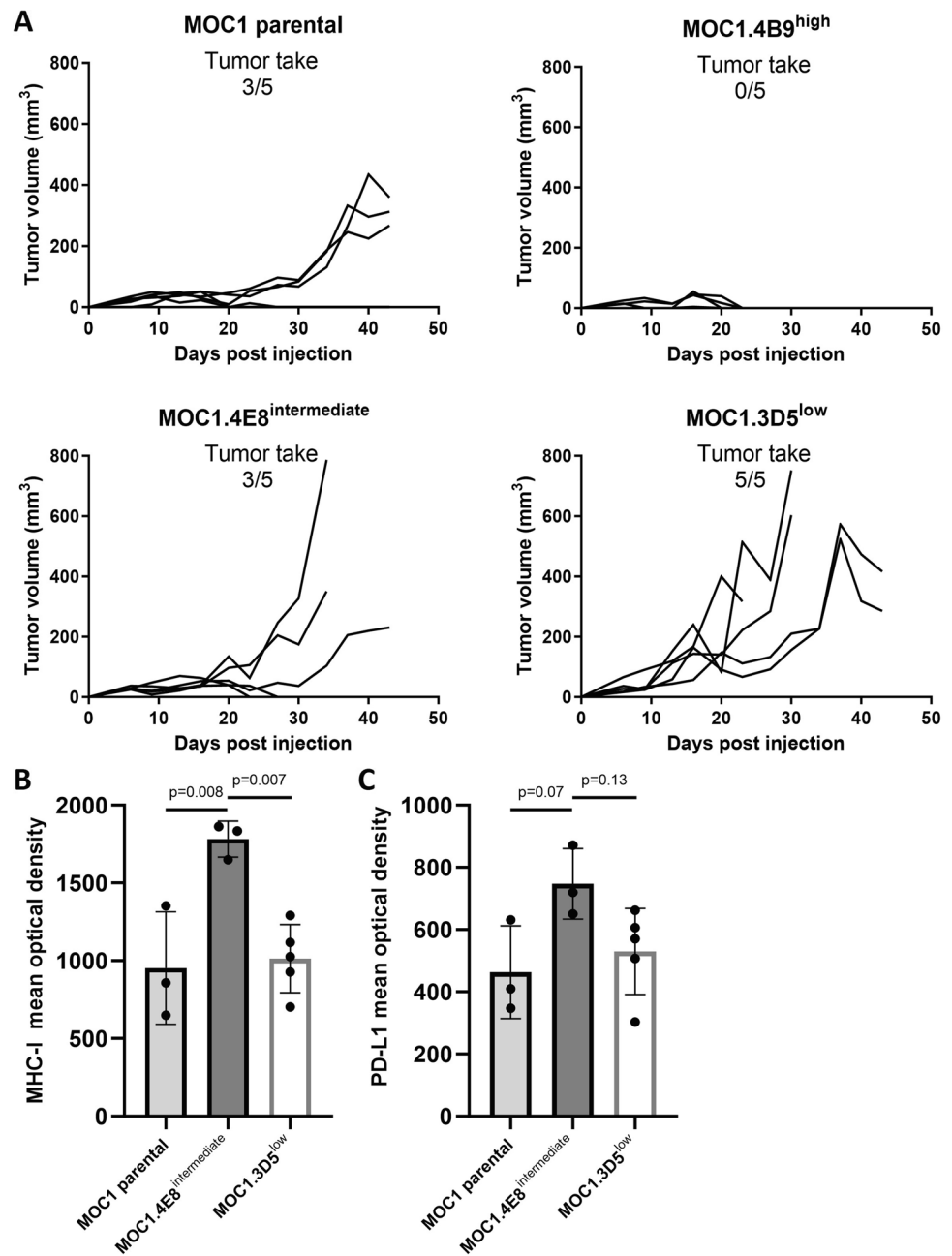
Radiotherapy Enhances Uptake of [¹¹¹In] In-anti-mPD-L1 in MOC1.3D5[low] Tumors

To investigate how radiotherapy affects tumor uptake of PD-L1 antibodies, [¹¹¹In]In-anti-mPD-L1 microSPECT/CT was performed in mice bearing irradiated (10 Gy single dose) or non-irradiated MOC1.3D5[low] tumors. Tumor, spleen and tumor-draining inguinal lymph nodes could be clearly distinguished on the PD-L1 microSPECT/CT image (Fig. 4A). A microSPECT/CT coronal view is provided in Supplementary Figure S7. Increased intensity of the [¹¹¹In]In-anti-mPD-L1 microSPECT signal was

observed in irradiated tumors compared to non-irradiated tumors, which was confirmed by ex vivo quantification of [¹¹¹In]In-anti-mPD-L1 uptake (16.8 ± 2.3 versus $13.8 \pm 2.0\%$ID/g, $p = 0.03$) (Fig. 4B). No difference in [¹¹¹In]In-anti-mPD-L1 uptake was observed in tumor-draining inguinal lymph node while a trend towards reduced [¹¹¹In]In-anti-mPD-L1 uptake in the spleen following irradiation was observed ($p = 0.06$). [¹¹¹In]In-anti-mPD-L1 uptake in the thymus was increased following irradiation ($p = 0.04$). To test if enhanced uptake of [¹¹¹In]In-anti-mPD-L1 could be a result of radiotherapy-enhanced perfusion, increased enhanced permeability
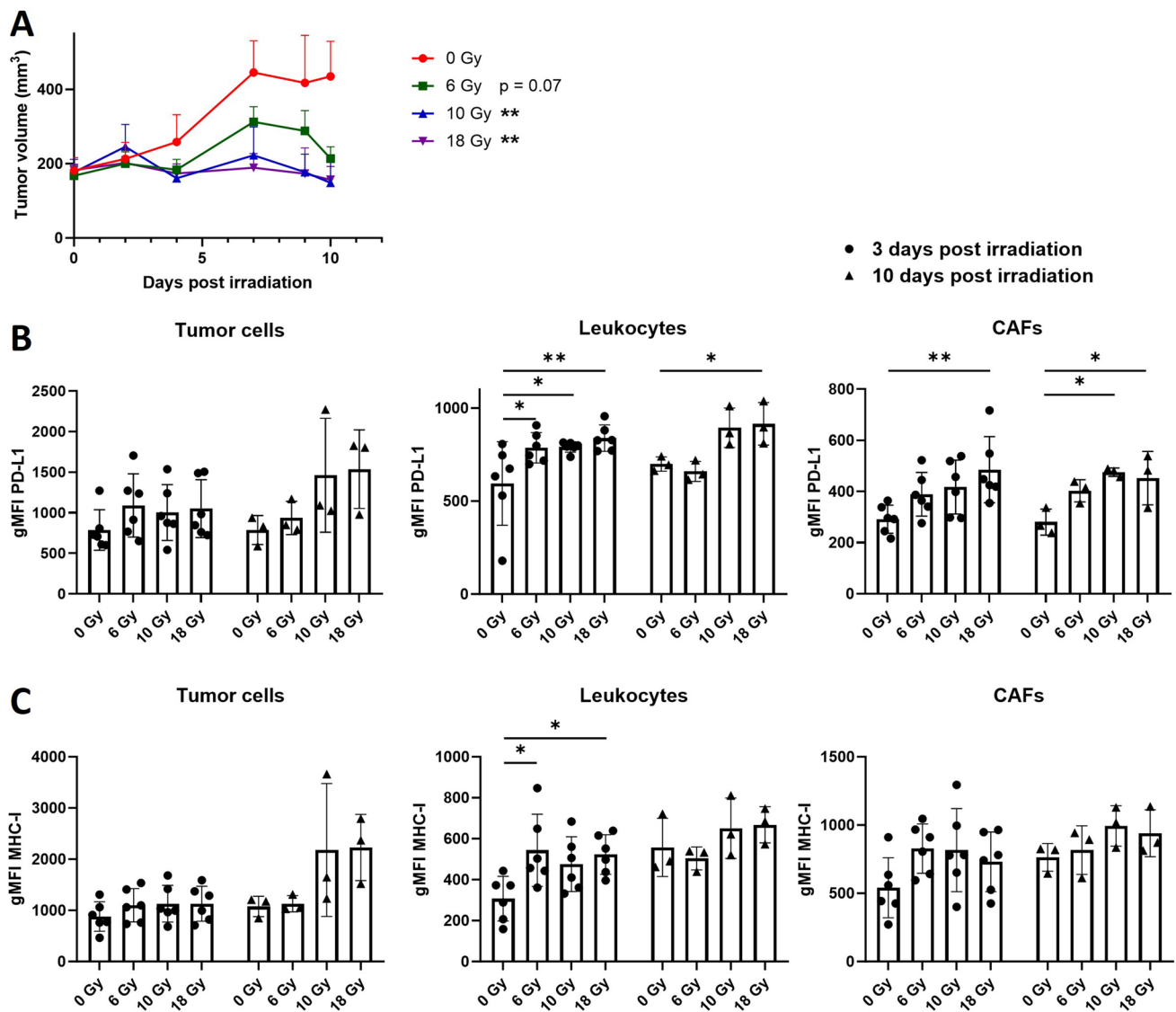
Fig. 3 Radiotherapy induces PD-L1 and MHC-I expression on several cell populations within the TME of MOC1.3D5^{low} tumors. (**A**) *In vivo* tumor growth of MOC1.3D5^{low} tumors after irradiation. Graph shows mean$\pm$SEM. (**B**) Geometric mean fluorescent intensity (gMFI) of PD-L1 signal and (**C**) gMFI of MHC-I signal on MOC1.3D5^{low}-derived CD45.2$^-$/EpCAM$^+$ tumor cells, CD45.2$^+$ leukocytes and CD45.2$^-$/EpCAM$^-$/CD90.1$^+$ CAFs. Graph bars show mean$\pm$SD

and retention effects, or influx of Fc receptor-positive immune cells, we performed a separate biodistribution study using an [^{111}In]In-IgG2b isotype control antibody. Irradiation did not increase the tumor uptake of [^{111}In]In-IgG2b (Supplementary tab. S1). Although the total tumor uptake of [^{111}In]In-IgG2b was higher than that of [^{111}In]In-anti-mPD-L1, this can be attributed to the slower blood clearance of [^{111}In]In-IgG2b because of the lack of "sink" organs such as the spleen [33, 37]. This is also reflected in the lower tumor-to-blood ratio of [^{111}In]In-IgG2b compared with [^{111}In]In-anti-mPD-L1. Complete biodistribution data are described in Supplementary Table. S1.

Autoradiography of tumor sections from mice injected with [^{111}In]In-anti-mPD-L1 showed a heterogenous [^{111}In]In-anti-mPD-L1 distribution, with increased tracer uptake in the tumor rim. IHC analysis shows that the tumor rim mostly consisted of CD45.2$^+$ immune cells, both for irradiated and non-irradiated tumors (Fig. 4C). Some PD-L1 expression was observed in EpCAM$^+$ tumor areas (Fig. 4D, yellow arrow), however most PD-L1 was present in the CD45.2$^+$ compartments of the TME as can be seen in 20$\times$ maginification images (Fig. 4D, white arrow). Moreover, the PD-L1 autoradiography signal correlated with both the CD45.2 signal (non irradiated: $\rho = 0.38 \pm 0.19$

Fig. 4 1×10 Gy irradiation increases [^{111}In]In-anti-mPD-L1 uptake in MOC1.3D5^{low} tumor tissue. (**A**) Maximum intensity projections of [^{111}In]In-anti-mPD-L1 microSPECT/CT in mice with non-irradiated and irradiated (1×10 Gy) tumors 24 h post tracer injection and 48 h post irradiation. Tumor (T), Spleen (S) and tumor-draining inguinal lymph node (LN) are indicated by white arrows. Scale indicating uptake in kBq/voxel. (**B**) Uptake of [^{111}In]In-anti-mPD-L1 in tumor, tumor-draining inguinal lymph node spleen and thymus of mice with non-irradiated and irradiated (1×10 Gy) tumors (%ID/g) 24 h post tracer injection and 48 h post irradiation. Graph bars show mean $\pm$ SD. (**C**) Autoradiography and IHC staining of PD-L1 (CD274, *red*), leukocytes (CD45.2, *blue*) and EpCAM (CD326, *green*) of the same tumor section of non-irradiated and irradiated (1×10 Gy) tumors. Scalebar represents 2.0 mm. (**D**) Color merge images of selected areas of non-irradiated and irradiated (1×10 Gy) tumors. PD-L1 (*red*), leukocytes (*blue*), EpCAM (*green*). White arrows indicate PD-L1$^+$/CD45.2$^+$ areas, yellow arrows indicate PD-L1$^+$/EpCAM$^+$ areas. White window in C indicates location of image on whole tumor section. $20 \times$ magnification, scalebar represents 100 μm
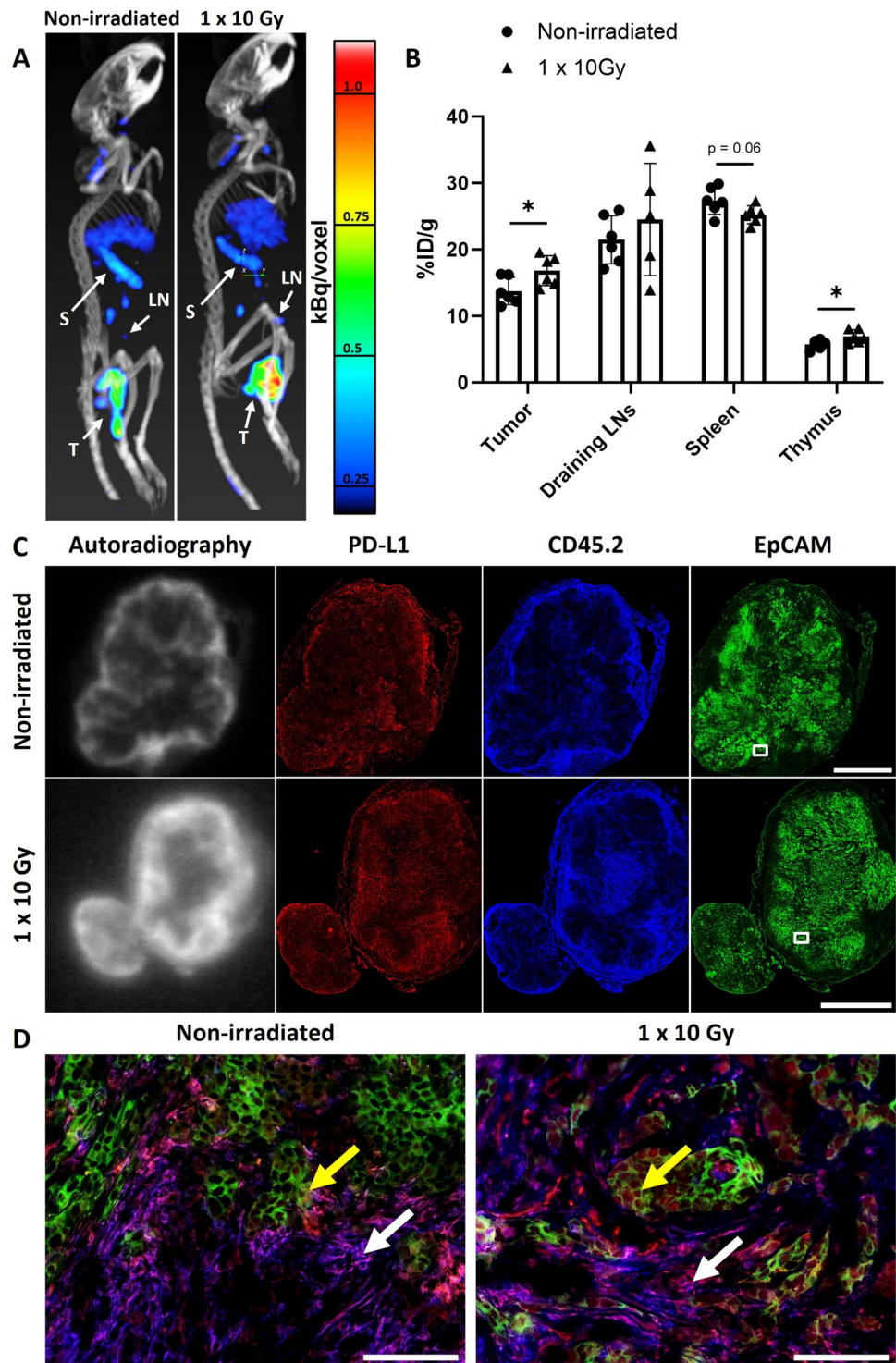
irradiated: $\rho = 0.26 \pm 0.19$) and the PD-L1 signal (non irradiated: $\rho = 0.34 \pm 0.14$ irradiated: $\rho = 0.35 \pm 0.09$) as determined by coregistration and quantitative analysis of autoradiography and IHC (Supplementary Fig. S8.). Further IHC analysis revealed co-localization of CD45.2 with MHC-II,

suggesting most leukocytes in this tumor are myeloid cells (Supplementary Fig. S9). Together, these findings show that PD-L1 expression is heterogeneous within the TME and, in line with the flow cytometry data, that radiotherapy induces PD-L1 expression in the MOC1.3D5^{low} TME.

Discussion

Radio- immunotherapy combination strategies are under investigation as a potential treatment option for HNSCC, but have not yet been proven effective [5, 7]. To optimize the efficacy and to steer optimal implementation of radio-immunotherapy into the clinic, in-depth knowledge on the mechanism of action is required. This can be obtained from well-characterized pre-clinical syngeneic mouse tumor models. In this study, we generate three clones derived from the syngeneic mouse oral cancer MOC1 and investigated the influence of immunological markers PD-L1 and MHC-I on tumor outgrowth and investigate the influence of radiotherapy on the TME of MOC1.3D5low.

In vitro analysis of MOC1-derived clones originating from the same parental cell line reveals a great heterogeneity in the inducibility of PD-L1 and MHC-I expression by IFNγ, while no differences are observed in their *in vitro* growth rate or radiosensitivity. This heterogeneity within a single model may affect processes such as anti-tumor immunity and consequently therapy response as in the real-life situation [26]. Although we characterized separate clones to develop a homogeneous and reproducible model to minimize the variation between experiments and the number of mice per study, it has to be noted that this is not a perfect reflection of the clinical situation where tumor heterogeneity is a general phenomenon.

Interestingly, the *in vitro* IFNγ-inducibility of PD-L1 and MHC-I correlates with tumor outgrowth. Mice inoculated with MOC1.3D5low showed consistent tumor outgrowth, while no tumor outgrowth was observed in MOC1.4B9high. These differences in tumor outgrowth might be a result of decreased IFNγ pathway gene expression (e.g. MHC-I and PD-L1), which is a well-known mechanism for immunotherapy resistance and decreased tumor outgrowth [26, 27]. Several other studies showed heterogeneity in tumor growth and therapy efficacy between single cell-derived clones from the same parental cell line that are dependent on tumor cell interactions with the immune-microenvironment [21, 38, 39]. In the tumors that developed from MOC1.4E8intermediate, MOC1.3D5low and the MOC1 parental cell line, no difference in infiltration of immune cells is detected, although this could not be investigated in MOC1.4B9high that did not grow out. Based on these observations it is unlikely that differences in immune cell infiltration are the reason for differences in tumor outgrowth. A possible mechanism explaining the consistent outgrowth of clone 3D5low could be the decreased recognition of the tumor cells by the immune system through its expression of MHC-I, as has been suggested in neuroblastoma and triple negative breast cancer [40, 41]. Whether decreased PD-L1 expression has a role

in increased tumor outgrowth remains controversial, as PD-L1 is an immunoregulatory pathway [26, 42].

The difference in expression of MHC-I and PD-L1 between MOC1.3D5low and MOC1.4E8intermediate *in vitro* is maintained after transplantation *in vivo* as assessed by IHC. Interestingly, contrary to its *in vitro* inducibility, also the (heterogenous) MOC1 parental cell line shows decreased expression of MHC-I and PD-L1 *in vivo*. This emphasizes that *in vitro* findings are not always translatable to the *in vivo* situation [43]. A potential explanation for this might be *in vivo* selection of the low MHC-I expressing cells that can grow out as they are not recognized by the immune system [44, 45].

In vitro irradiation of MOC1.3D5low cells increases the expression of PD-L1 and MHC-I. Flow cytometry analysis of MOC1.3D5low tumors also shows upregulation of PD-L1 on leukocytes (CD45.2+) and CAFs (EpCAM−/CD45.2−/CD90.1+) and upregulation of MHC-I on leukocytes after irradiation. As CD90.1 can be expressed on multiple cell types including endothelial cells and pericytes, we cannot exclude that these cell types contribute to the observed PDL1 signal [46, 47]. However, because CAFs make up a significant part of the TME in HNSSC, and CD90.1 is an emerging marker for CAFs, we assume the CD45.2−/EpCAM−/CD90.1+ population to consist mainly of CAFs [48, 49]. A marker that could be used to further characterize CAFs is fibroblast activation protein (FAP) that is also targeted for PET imaging of cancer [50].

[111In]In-anti-mPD-L1 microSPECT/CT imaging of MOC1.3D5low tumors shows increased tracer uptake in irradiated compared to non-irradiated tumors. Higher tracer uptake is observed at the tumor rim compared to the core. IHC analysis reveals that this uptake correlates with stroma that is highly infiltrated by CD45.2+ leukocytes. Albeit at lower intensity, also EpCAM+ tumor areas exhibit PD-L1 expression, revealing PD-L1 expression by different cell populations throughout the TME [51]. The small reduction of [111In]In-anti-mPD-L1 uptake in spleen following irradiation was not observed in other tumor models, but could be the result of migration of leukocytes towards the tumor [34]. Our findings show that radiotherapy not only enhances PD-L1 and MHC-I expression on tumor cells, as observed in other studies, but also on several other, non-tumor cell populations within the TME [34, 52]. These radiation-induced changes could potentially serve as a target when radiotherapy is combined with immunotherapy. An example of such a change could be the upregulation of PD-L1 expression on host cells, which is suggested to be essential for immunotherapy efficiency [37, 53]. Moreover, other studies show upregulation of different immune checkpoints like VISTA, TIM-3 and PD-1 in HNSCC and immune cells following

irradiation, potentially contributing to immunotherapy efficacy against these targets [54–56]. Imaging of PD-L1 and other immune checkpoints at different time points after radiotherapy, preferably using radiotracers with a short half-life labeled with a positron-emitting radionuclide to enable PET imaging, could potentially show these dynamic expression levels in patients [57]. Further analysis of subsets of immune cells and CAFs, or analysis of different aspects of the environment (e.g. hypoxic areas, tumor stroma, etc.), might reveal different responses to irradiation within these cell populations and environments that might provide a reasoning for immune- radiotherapy combination strategies [36, 58].

The kinetics of radiation-induced changes on the TME could provide a rationale to determine the optimal timing of immunotherapy administration and supports longitudinal monitoring during therapy, for instance by PD-L1 imaging. It is suggested that concurrent radio- immunotherapy, generally applied in most HNSCC trials, might potentially be counter-effective as tissue-resident immune cells are irradiated during the course of treatment and thereby die as a result. We and others show that PD-L1 and MHC-I are upregulated at least up to 10 days post irradiation [11]. Immunotherapy administration after radiotherapy, sparing activated immune cells, might therefore be preferable as has been successful in non-small-cell lung cancer [59].

Conclusions

In summary, MOC1.3D5^{low} shows consistent and high tumor take and is a reproducible syngeneic mouse model for radiotherapy and immunotherapy research. Stable tumor outgrowth is correlated with decreased inducibility of PD-L1 and MHC-I in MOC1-derived clones. Lastly, PD-L1 and MHC-I is expressed on multiple cell populations within the TME as observed by flow cytometry, and can be upregulated by radiotherapy in several subsets of cells. Moreover, an increased tumor uptake of [^{111}In]In-anti-mPD-L1 was seen following radiotherapy. This knowledge can help to optimize radio- immunotherapy combination strategies (e.g. timing) in HNSCC and longitudinal assessment of the TME by means of PD-L1 imaging may serve as a biomarker in clinical translation.

Author Contributions Conceptualization: DB, GS, MA, RvdB, PS, GA, SH, JB.
Formal analysis: DB, GS, RvdB.
Funding acquisition: SH, JB.
Investigation: DB, GS, MA, RvdB, JP.
Supervision: PS, GA, SH, JB.
Writing—original draft: DB.
Writing—review and editing: GS, MA, RvdB, JP, PS, GA, SH, JB.

Declarations

References

1. Chow LQM (2020) Head and Neck Cancer. N Engl J Med 382(1):60–72
2. Kamangar F, Dores GM, Anderson WF (2006) Patterns of cancer incidence, mortality, and prevalence across five continents: defining priorities to reduce cancer disparities in different geographic regions of the world. J Clin Oncol 24(14):2137–2150
3. Gaipl US, Multhoff G, Scheithauer H, Lauber K, Hehlgans S, Frey B, Rödel F (2014) Kill and spread the word: stimulation of antitumor immune responses in the context of radiotherapy. Immunotherapy 6(5):597–610
4. Qian JM, Schoenfeld JD (2020) Radiotherapy and immunotherapy for head and neck cancer: current evidence and challenges. Front Oncol 10:608772
5. Lee NY, Ferris RL, Psyrri A, Haddad RI, Tahara M, Bourhis J et al (2021) Avelumab plus standard-of-care chemoradiotherapy versus chemoradiotherapy alone in patients with locally advanced squamous cell carcinoma of the head and neck: a randomised, double-blind, placebo-controlled, multicentre, phase 3 trial. Lancet Oncol 22(4):450–462
6. Tao Y, Auperin A, Sun X, Sire C, Martin L, Coutte A et al (2020) Avelumab-cetuximab-radiotherapy versus standards of care in locally advanced squamous-cell carcinoma of the head and neck: The safety phase of a randomised phase III trial GORTEC 2017–01 (REACH). Eur J Cancer 141:21–29
7. Tao Y, Biau J, Sun XS, Sire C, Martin L, Alfonsi M et al (2023) Pembrolizumab versus cetuximab concurrent with radiotherapy in patients with locally advanced squamous cell carcinoma of head and neck unfit for cisplatin (GORTEC 2015–01

PembroRad): a multicenter, randomized, phase II trial. Ann Oncol 34(1):101–110

8. Machiels JP, Tao Y, Burtness B, Tahara M, Licitra L, Rischin D et al (2020) Pembrolizumab given concomitantly with chemoradiation and as maintenance therapy for locally advanced head and neck squamous cell carcinoma: KEYNOTE-412. Future Oncol 16(18):1235–1243

9. Darragh LB, Gadwa J, Pham TT, Van Court B, Neupert B, Olimpo NA et al (2022) Elective nodal irradiation mitigates local and systemic immunity generated by combination radiation and immunotherapy in head and neck tumors. Nat Commun 13(1):7015

10. Saddawi-Konefka R, O'Farrell A, Faraji F, Clubb L, Allevato MM, Jensen SM et al (2022) Lymphatic-preserving treatment sequencing with immune checkpoint inhibition unleashes cDC1-dependent antitumor immunity in HNSCC. Nat Commun 13(1):4298

11. Morisada M, Clavijo PE, Moore E, Sun L, Chamberlin M, Van Waes C et al (2018) PD-1 blockade reverses adaptive immune resistance induced by high-dose hypofractionated but not low-dose daily fractionated radiation. Oncoimmunology 7(3):e1395996

12. Oweida A, Lennon S, Calame D, Korpela S, Bhatia S, Sharma J et al (2017) Ionizing radiation sensitizes tumors to PD-L1 immune checkpoint blockade in orthotopic murine head and neck squamous cell carcinoma. Oncoimmunology 6(10):e1356153

13. Oweida A, Hararah MK, Phan A, Binder D, Bhatia S, Lennon S et al (2018) Resistance to radiotherapy and PD-L1 blockade is mediated by TIM-3 upregulation and regulatory T-cell infiltration. Clin Cancer Res 24(21):5368–5380

14. Kim SS, Shen S, Miyauchi S, Sanders PD, Franiak-Pietryga I, Mell L et al (2020) B cells improve overall survival in HPV-associated squamous cell carcinomas and are activated by radiation and PD-1 blockade. Clin Cancer Res 26(13):3345–3359

15. Newton JM, Hanoteau A, Liu HC, Gaspero A, Parikh F, Gartrell-Corrado RD et al (2019) Immune microenvironment modulation unmasks therapeutic benefit of radiotherapy and checkpoint inhibition. J Immunother Cancer 7(1):216

16. Hanoteau A, Newton JM, Krupar R, Huang C, Liu HC, Gaspero A et al (2019) Tumor microenvironment modulation enhances immunologic benefit of chemoradiotherapy. J Immunother Cancer 7(1):10

17. Xiao R, Allen CT, Tran L, Patel P, Park SJ, Chen Z et al (2018) Antagonist of cIAP1/2 and XIAP enhances anti-tumor immunity when combined with radiation and PD-1 blockade in a syngeneic model of head and neck cancer. Oncoimmunology 7(9):e1471440

18. Patin EC, Dillon MT, Nenclares P, Grove L, Soliman H, Leslie I et al (2022) Harnessing radiotherapy-induced NK-cell activity by combining DNA damage-response inhibition and immune checkpoint blockade. J Immunother Cancer 10(3):e004306

19. Ansems M, Span PN (2020) The tumor microenvironment and radiotherapy response; a central role for cancer-associated fibroblasts. Clin Transl Radiat Oncol 22:90–97

20. de Visser KE, Joyce JA (2023) The evolving tumor microenvironment: From cancer initiation to metastatic outgrowth. Cancer Cell 41(3):374–403

21. Xu BL, Wang XM, Chen GY, Yuan P, Han L, Qin P et al (2022) *In vivo* growth of subclones derived from lewis lung carcinoma is determined by the tumor microenvironment. Am J Cancer Res 12(11):5255–5270

22. Yoo SH, Keam B, Ock CY, Kim S, Han B, Kim JW et al (2019) Prognostic value of the association between MHC class I downregulation and PD-L1 upregulation in head and neck squamous cell carcinoma patients. Sci Rep 9(1):7680

23. Sanchez-Canteli M, Granda-Diaz R, Del Rio-Ibisate N, Allonca E, Lopez-Alvarez F, Agorreta J et al (2020) PD-L1 expression correlates with tumor-infiltrating lymphocytes and better prognosis

in patients with HPV-negative head and neck squamous cell carcinomas. Cancer Immunol Immunother 69(10):2089–2100

24. Zhou Z, Mu D, Zhang D, Zhang X, Ding X, Yang J et al (2020) PD-L1 in combination with CD8+ TIL and HIF-1α are promising prognosis predictors of head and neck squamous cell carcinoma. Cancer Manag Res 12:13233–13239

25. Wuerdemann N, Gültekin SE, Pütz K, Wittekindt C, Huebbers CU, Sharma SJ et al (2020) PD-L1 expression and a high tumor infiltrate of CD8+ lymphocytes predict outcome in patients with oropharyngeal squamous cells carcinoma. Int J Mol Sci 21(15):5228

26. Williams JB, Li S, Higgs EF, Cabanov A, Wang X, Huang H, Gajewski TF (2020) Tumor heterogeneity and clonal cooperation influence the immune selection of IFN-gamma-signaling mutant cancer cells. Nat Commun 11(1):602

27. Gao J, Shi LZ, Zhao H, Chen J, Xiong L, He Q et al (2016) Loss of IFN-γ pathway genes in tumor cells as a mechanism of resistance to anti-CTLA-4 therapy. Cell 167(2):397-404 e9

28. Kono M, Saito S, Egloff AM, Allen CT, Uppaluri R (2022) The mouse oral carcinoma (MOC) model: A 10-year retrospective on model development and head and neck cancer investigations. Oral Oncol 132:106012

29. Morisada M, Moore EC, Hodge R, Friedman J, Cash HA, Hodge JW et al (2017) Dose-dependent enhancement of T-lymphocyte priming and CTL lysis following ionizing radiation in an engineered model of oral cancer. Oral Oncol 71:87–94

30. Joiner M, van der Kogel AJ (2018) Basic clinical radiobiology, 5th edn. CRC Press

31. Meijer TWH, Peeters WJM, Dubois LJ, van Gisbergen MW, Biemans R, Venhuizen JH et al (2018) Targeting glucose and glutamine metabolism combined with radiation therapy in non-small cell lung cancer. Lung Cancer 126:32–40

32. van den Bijgaart RJE, Kroesen M, Brok IC, Reijnen D, Wassink M, Boon L et al (2020) Anti-GD2 antibody and Vorinostat immunocombination therapy is highly effective in an aggressive orthotopic neuroblastoma model. Oncoimmunology 9(1):1817653

33. Sandker GGW, Adema G, Molkenboer-Kuenen J, Wierstra P, Bussink J, Heskamp S, Aarntzen E (2022) PD-L1 antibody pharmacokinetics and tumor targeting in Mouse models for infectious diseases. Front Immunol 13:837370

34. Heskamp S, Wierstra PJ, Molkenboer-Kuenen JDM, Sandker GW, Thordardottir S, Cany J et al (2019) PD-L1 microSPECT/CT imaging for longitudinal monitoring of PD-L1 expression in syngeneic and humanized mouse models for cancer. Cancer Immunol Res 7(1):150–161

35. Rademakers SE, Rijken PF, Peeters WJ, Nijkamp MM, Barber PR, van der Laak J et al (2011) Parametric mapping of immunohistochemically stained tissue sections; a method to quantify the colocalization of tumor markers. Cell Oncol 34(2):119–129

36. Boreel DF, Span PN, Kip A, Boswinkel M, Peters JPW, Adema GJ et al (2023) Quantitative Imaging of Hypoxic CAIX-Positive Tumor Areas with Low Immune Cell Infiltration in Syngeneic Mouse Tumor Models. Mol Pharm 20(4):2245–2255

37. Tang H, Liang Y, Anders RA, Taube JM, Qiu X, Mulgaonkar A et al (2018) PD-L1 on host cells is essential for PD-L1 blockade-mediated tumor regression. J Clin Invest 128(2):580–588

38. Kroesen M, Nierkens S, Ansems M, Wassink M, Orentas RJ, Boon L et al (2014) A transplantable TH-MYCN transgenic tumor model in C57Bl/6 mice for preclinical immunological studies in neuroblastoma. Int J Cancer 134(6):1335–1345

39. Remels LM, De Baetselier PC (1987) Characterization of 3LL-tumor variants generated by *in vitro* macrophage-mediated selection. Int J Cancer 39(3):343–352

40. Neal ZC, Imboden M, Rakhmilevich AL, Kim KM, Hank JA, Surfus J et al (2004) NXS2 murine neuroblastomas express increased levels of MHC class I antigens upon recurrence following

NK-dependent immunotherapy. Cancer Immunol Immunother 53(1):41–52

41. Lee JV, Housley F, Yau C, Nakagawa R, Winkler J, Anttila JM et al (2022) Combinatorial immunotherapies overcome MYC-driven immune evasion in triple negative breast cancer. Nat Commun 13(1):3671

42. Kleinovink JW, Marijt KA, Schoonderwoerd MJA, van Hall T, Ossendorp F, Fransen MF (2017) PD-L1 expression on malignant cells is no prerequisite for checkpoint therapy. Oncoimmunology 6(4):e1294299

43. Otava M, Shkedy Z, Talloen W, Verheyen GR, Kasim A (2015) Identification of *in vitro* and *in vivo* disconnects using transcriptomic data. BMC Genom 16(1):615

44. Khong HT, Restifo NP (2002) Natural selection of tumor variants in the generation of "tumor escape" phenotypes. Nat Immunol 3(11):999–1005

45. Dhatchinamoorthy K, Colbert JD, Rock KL (2021) Cancer immune evasion through loss of MHC class I antigen presentation. Front Immunol 12:636568

46. Wetzel A, Chavakis T, Preissner KT, Sticherling M, Haustein UF, Anderegg U, Saalbach A (2004) Human Thy-1 (CD90) on Activated Endothelial Cells Is a Counterreceptor for the Leukocyte Integrin Mac-1 (CD11b/CD18)1. J Immunol 172(6):3850–3859

47. Bradley JE, Ramirez G, Hagood JS (2009) Roles and regulation of Thy-1, a context-dependent modulator of cell phenotype. BioFactors 35(3):258–265

48. Kumar D, New J, Vishwakarma V, Joshi R, Enders J, Lin F et al (2018) Cancer-associated fibroblasts drive glycolysis in a targetable signaling loop implicated in head and neck squamous cell carcinoma progression. Cancer Res 78(14):3769–3782

49. Zhao Z, Li T, Yuan Y, Zhu Y (2023) What is new in cancer-associated fibroblast biomarkers? Cell Commun Signal 21(1):96

50. Prive BM, Boussihmad MA, Timmermans B, van Gemert WA, Peters SMB, Derks YHW et al (2023) Fibroblast activation protein-targeted radionuclide therapy: background, opportunities, and challenges of first (pre)clinical studies. Eur J Nucl Mol Imaging 50(7):1906–1918

51. Qiao XW, Jiang J, Pang X, Huang MC, Tang YJ, Liang XH, Tang YL (2020) The evolving landscape of PD-1/PD-L1 pathway in head and neck cancer. Front Immunol 11:1721

52. Reits EA, Hodge JW, Herberts CA, Groothuis TA, Chakraborty M, Wansley EK et al (2006) Radiation modulates the peptide repertoire, enhances MHC class I expression, and induces successful antitumor immunotherapy. J Exp Med 203(5):1259–1271

53. Lin H, Wei S, Hurt EM, Green MD, Zhao L, Vatan L et al (2018) Host expression of PD-L1 determines efficacy of PD-L1 pathway blockade-mediated tumor regression. J Clin Invest 128(2):805–815

54. Makowska A, Lelabi N, Nothbaum C, Shen L, Busson P, Tran TTB et al (2021) Radiotherapy combined with PD-1 inhibition increases NK cell cytotoxicity towards nasopharyngeal carcinoma cells. Cells 10(9):2458

55. Li D, Chen R, Wang YW, Fornace AJ Jr, Li HH (2018) Prior irradiation results in elevated programmed cell death protein 1 (PD-1) in T cells. Int J Radiat Biol 94(5):488–494

56. Wang L, Wang S, Zhang J, Peng J, Cheng B, Li H, Hu Q (2023) Radiotherapy upregulated immune checkpoints contribute to the development of second primary OSCC. Oral Dis 30(4):2188–2201

57. Yang H, Zeng X, Liu J, Wen X, Liu H, Liang Y et al (2024) Development of small-molecular-based radiotracers for PET imaging of PD-L1 expression and guiding the PD-L1 therapeutics. Eur J Nucl Med Mol Imaging 51:1582–1592

58. Menon H, Ramapriyan R, Cushman TR, Verma V, Kim HH, Schoenhals JE et al (2019) Role of radiation therapy in modulation of the tumor stroma and microenvironment. Front Immunol 10:193

59. Antonia SJ, Villegas A, Daniel D, Vicente D, Murakami S, Hui R et al (2017) Durvalumab after chemoradiotherapy in stage III non–small-cell lung cancer. N Engl J Med 377(20):1919–1929